High-throughput small molecule screen identifies inhibitors of aberrant chromatin accessibility

Samantha G. Pattenden[a,b,1], Jeremy M. Simon[c,d,e,1], Aminah Wali[c,d,f,1], Chatura N. Jayakody[a,b], Jacob Troutman[d,g], Andrew W. McFadden[d], Joshua Wooten[c,d,f], Cameron C. Wood[a,b], Stephen V. Frye[a,b], William P. Janzen[a,b,2], and Ian J. Davis[c,d,g,h,3]

[a]Center for Integrative Chemical Biology and Drug Discovery, University of North Carolina at Chapel Hill, Chapel Hill, NC 27302; [b]Division of Chemical Biology and Medicinal Chemistry, Eshelman School of Pharmacy, University of North Carolina at Chapel Hill, Chapel Hill, NC 27302; [c]Department of Genetics, School of Medicine, University of North Carolina at Chapel Hill, Chapel Hill, NC 27599; [d]Lineberger Comprehensive Cancer Center, School of Medicine, University of North Carolina at Chapel Hill, Chapel Hill, NC 27599; [e]Curriculum in Bioinformatics and Computational Biology, University of North Carolina at Chapel Hill, Chapel Hill, NC 27599; [f]Curriculum in Genetics and Molecular Biology, University of North Carolina at Chapel Hill, Chapel Hill, NC 27599; [g]Department of Pediatrics, School of Medicine, University of North Carolina at Chapel Hill, Chapel Hill, NC 27599; and [h]Carolina Center for Genome Sciences, School of Medicine, University of North Carolina at Chapel Hill, Chapel Hill, NC 27599

Edited by Steven Henikoff, Fred Hutchinson Cancer Research Center, Seattle, WA, and approved January 21, 2016 (received for review November 4, 2015)

Mutations in chromatin-modifying proteins and transcription factors are commonly associated with a wide variety of cancers. Through gain- or loss-of-function, these mutations may result in characteristic alterations of accessible chromatin, indicative of shifts in the landscape of regulatory elements genome-wide. The identification of compounds that reverse a specific chromatin signature could lead to chemical probes or potential therapies. To explore whether chromatin accessibility could serve as a platform for small molecule screening, we adapted formaldehyde-assisted isolation of regulatory elements (FAIRE), a chemical method to enrich for nucleosome-depleted genomic regions, as a high-throughput, automated assay. After demonstrating the validity and robustness of this approach, we applied this method to screen an epigenetically targeted small molecule library by evaluating regions of aberrant nucleosome depletion mediated by EWSR1-FLI1, the chimeric transcription factor critical for the bone and soft tissue tumor Ewing sarcoma. As a class, histone deacetylase inhibitors were greatly overrepresented among active compounds. These compounds resulted in diminished accessibility at targeted sites by disrupting transcription of EWSR1-FLI1. Capitalizing on precise differences in chromatin accessibility for drug discovery efforts offers significant advantages because it does not depend on the a priori selection of a single molecular target and may detect novel biologically relevant pathways.

chromatin | Ewing sarcoma | high throughput screening | FAIRE | histone deacetylase inhibitor

A growing range of human cancers have been associated with mutations in genes encoding proteins that regulate chromatin, the assembly of proteins and DNA that control DNA-templated processes, including transcription and replication (1, 2). Small molecule drugs and chemical probes offer an approach to explore the biological consequences of these mutations and are emerging as a therapeutic strategy to target disease pathways. Drugs targeting histone deacetylase (HDAC) enzymes, the bromodomain reader BRD4, and DNA methylation have already received regulatory approval or have entered clinical testing, and chemical probes have been developed against a broad range of chromatin regulators, such as the methyltransferases (3) DOT1L (4), EZH2 (5–8), and G9a (9, 10), and the reader proteins L3MBTL3 (11) and BRD4 (12–14). However, transcription factors that lack enzymatic activity or binding pockets with targetable molecular features have been considered "undruggable," and a reductionist approach based on identification of their molecular targets has largely failed.

The majority of Ewing sarcomas, highly malignant pediatric bone and soft tissue tumors, harbor a chromosomal translocation that joins the amino-terminal domain of *EWSR1* with the DNA binding domain of the ETS transcription factor family member *FLI1* to generate the chimeric transcription factor EWSR1-FLI1 (15). Translocations with other ETS genes are detected in most of the remaining tumors, yielding similarly functioning fusion proteins (16). We recently found that, despite conservation of the ETS DNA binding domain, the fusion oncoprotein uniquely localizes to specific microsatellite regions (17, 18). Using formaldehyde-assisted isolation of regulatory elements (FAIRE), a biochemical strategy to enrich for nucleosome-depleted regions of chromatin, we demonstrated that EWSR1-FLI1 binding was necessary to maintain nucleosome depletion at these sites. The mechanism through which EWSR1-FLI1 modifies chromatin remains unknown. Because EWSR1-FLI1 does not possess recognizable catalytic activity, other yet-to-be-identified proteins likely mediate its ability to remodel chromatin.

The absence of a biochemical mechanism would typically pose challenges for chemical targeting. However, we hypothesized that reversing a unique chromatin signature could serve as a strategy to discover small molecules with activity toward EWSR1-FLI1. To target this activity, we adapted and validated FAIRE as an automated, high-throughput tool and applied this method to

Significance

Transcriptional regulators lacking enzymatic activity or binding pockets with targetable molecular features have typically been considered "undruggable," and a reductionist approach based on identification of their molecular targets has largely failed. We have demonstrated that the Ewing sarcoma chimeric transcription factor, EWSR1-FLI1, maintains accessible chromatin at disease-specific regions. We adapted formaldehyde-assisted isolation of regulatory elements (FAIRE), an assay for accessible chromatin, to screen an epigenetically targeted small molecule library for compounds that reverse the disease-associated signature. This approach can be applied broadly for discovery of chromatin-based developmental therapeutics and offers significant advantages because it does not require the selection of a single molecular target. Using this approach, we identified a specific class of compounds with therapeutic potential.

Author contributions: S.G.P., J.M.S., S.V.F., W.P.J., and I.J.D. designed research; S.G.P., J.M.S., A.W., C.N.J., J.T., A.W.M., J.W., and C.C.W. performed research; S.V.F. contributed new reagents/analytic tools; S.G.P., J.M.S., A.W., C.N.J., J.T., A.W.M., J.W., W.P.J., and I.J.D. analyzed data; and S.G.P., J.M.S., A.W., S.V.F., W.P.J., and I.J.D. wrote the paper.

The authors declare no conflict of interest.

This article is a PNAS Direct Submission.

Data deposition: The data reported in this paper have been deposited in the Gene Expression Omnibus (GEO) database, www.ncbi.nlm.nih.gov/geo (accession no. GSE61735).

[1]S.G.P., J.M.S., and A.W. contributed equally to this work.

[2]Present address: Epizyme Inc., Cambridge, MA 02139.

[3]To whom correspondence should be addressed. Email: ian_davis@med.unc.edu.

This article contains supporting information online at www.pnas.org/lookup/suppl/doi:10.1073/pnas.1521827113/-/DCSupplemental.

evaluate a focused set of small molecules designed to interact with proteins that regulate chromatin. Because this approach directly assessed the effects of compounds on a specific, disease-associated aberrant chromatin signature, while remaining agnostic about precise molecular mechanisms, it enabled the discovery of agents that affect the underlying molecular defect without requiring an a priori selection of molecular targets.

Results

Validation of Column-Based FAIRE. As currently applied, FAIRE, a biochemical assay for the enrichment of nucleosome-depleted regions of the genome, is dependent on organic extraction with a mixture of phenol and chloroform. Because this critical extraction step is not easily automated, we adapted and miniaturized FAIRE by substituting organic extraction with solid-phase selection and robotic automation, hereafter termed high-throughput FAIRE (HT-FAIRE) (Fig. 1*A*). Because the chromatin fractionation step is central to this technique, we compared the performance of these methods. Quantitative locus-specific testing demonstrated that both approaches offered concordant enrichment at a series of promoter and enhancer regions (Fig. S1). We then compared the performance of both methods genome-wide. We used primary human umbilical vein endothelial cells (HUVECs) since multiple genomic datasets exploring chromatin features have been generated for these cells permitting subsequent integrative analyses of the FAIRE results [Encyclopedia of DNA Elements (ENCODE) Tier 2] (19). HT-FAIRE demonstrated signal enrichment patterns similar to those observed using standard FAIRE. For example, enrichment at transcriptional start sites (TSSs), including positive correlation with RNA abundance as well as enrichment at CCCTC-binding factor (CTCF) sites demonstrated similar characteristics as previously reported FAIRE studies (Fig. 1 *B–D*) (20). Signal enrichment by HT-FAIRE was less robust at TSSs, consistent with the quantitative PCR (qPCR) results. Of the top 10,000 nucleosome-depleted regions detected in HUVECs by HT-FAIRE, ∼90% overlapped those sites identified by standard FAIRE. In contrast, fewer than 50% of enriched regions overlapped FAIRE sites from any of six other cell lines (Fig. S2*A*), demonstrating that HT-FAIRE offers a level of specificity similar to that reported in previous studies (21).

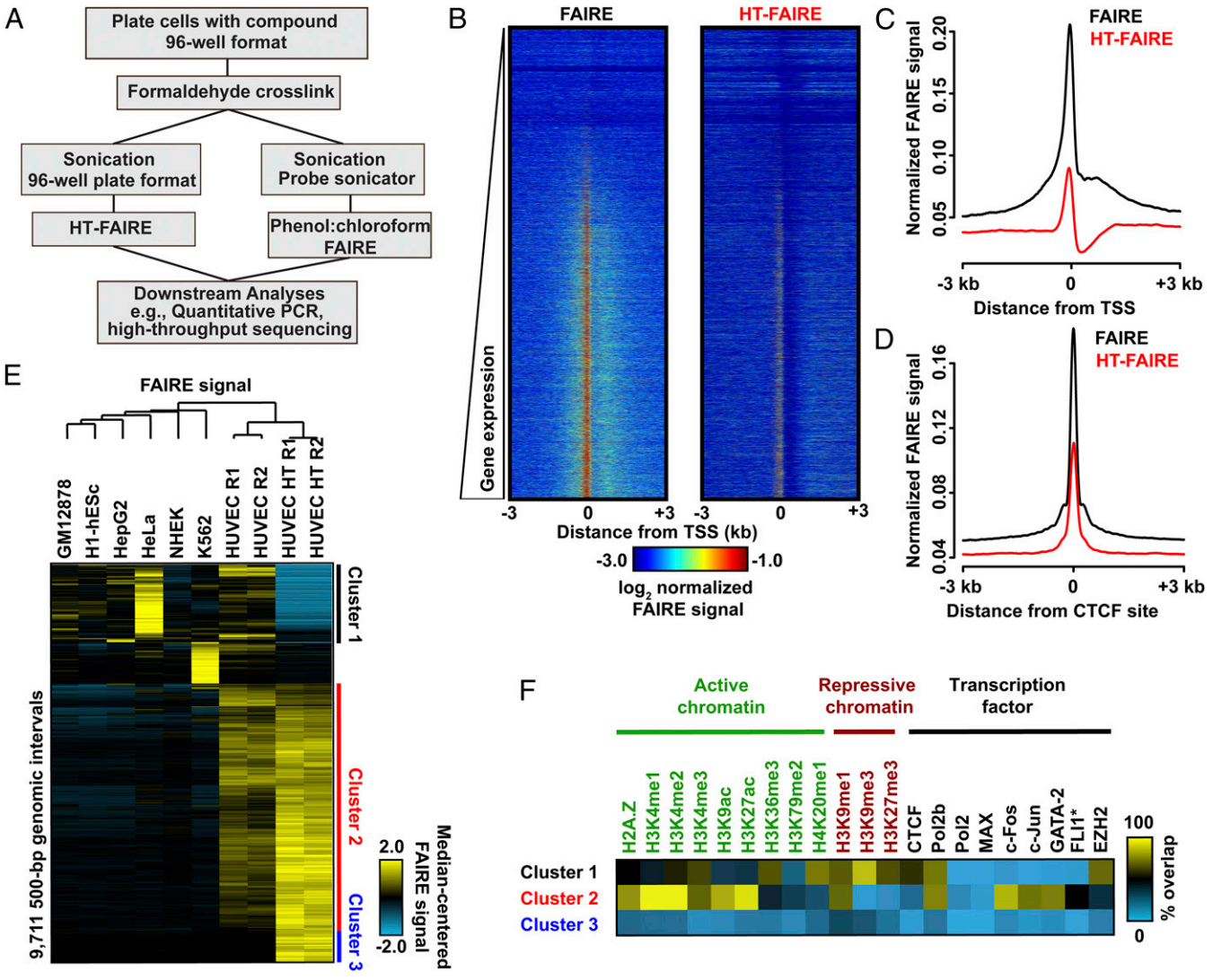

Fig. 1. Comparison of FAIRE methodologies. (*A*) Flow diagram comparing column-based and standard FAIRE methods. (*B*) Heatmap representation of normalized FAIRE enrichment (±3 kb from TSS) using standard (*Left*) or column (*Right*) FAIRE in HUVEC. (*C*) Normalized FAIRE signal from both methods ±3 kb from TSS. (*D*) Normalized FAIRE signal from both methods ±3 kb around HUVEC CTCF sites (ENCODE). (*E*) Hierarchical clustering analysis of 500-bp intervals demonstrating differential FAIRE signals across seven cell types, as well as HUVEC HT-FAIRE. Platform-specific (clusters 1 and 3) and cell type-specific (cluster 2) clusters were identified. (*F*) Fractional overlap annotation of clusters 1–3, with histone modifications and transcription factors (ENCODE).

We then examined those genomic regions that most discriminate HT-FAIRE and standard FAIRE and also demonstrate HUVEC cell-type specificity. Hierarchical clustering of these ~9,700 genomic regions identified three groups (Fig. 1*E*). Cluster 1 (1,805 regions) consisted of those regions enriched in all cell lines when assayed by standard FAIRE but not by HT-FAIRE. Cluster 2 (6,017 regions), by far the largest, consisted of regions with HUVEC-specific signal enrichment that was detected by both HT-FAIRE and standard FAIRE. Cluster 3 (843 regions) consisted of regions selectively identified by HT-FAIRE. Regions in each cluster were then associated with genes [Genome Regions Enrichment of Annotations Tool (GREAT)] (22). As expected, the HUVEC-selective sites detected by both HT-FAIRE and standard FAIRE (cluster 2) were tightly linked with endothelial cell ontologies, including angiogenesis ($q = 4.4 \times 10^{-12}$) and regulation of cell-substrate adhesion ($q = 6.5 \times 10^{-7}$) (Fig. S2*B*). No significant gene ontologies were associated with the regions in the other clusters. To test whether FAIRE-enriched regions were likely to harbor regulatory elements, we annotated the sites from each cluster with active and repressive histone modifications. We also tested for association with targeting of numerous transcription factors, including those known to be important in endothelial cell biology, as assessed by ChIP-seq (17, 19). (Fig. 1*F*). Sites in cluster 2 (common to both platforms, HUVEC-specific) were associated primarily with active histone modifications, as well as sites targeted by FLI1, FOS, JUN, GATA2, and RNA Polymerase II. The prevalence of putative FLI1 and FOS/JUN binding sites was corroborated by the enrichment of ETS and AP1 DNA sequence motifs in these regions ($P < 1 \times 10^{-800}$) (Fig. S2*C*). ETS (specifically ETV2) and AP1 factors are both known to play prominent roles in endothelial development (23, 24). Regions in cluster 1 were more closely associated with repressive modifications and EZH2 binding (Fig. 1*F*). Clusters 1 and 3 were distinguished by enrichment for repetitive regions, with each cluster associated with a specific repetitive element class: satellites (82% of cluster 1 sites) and simple repeats (71% of cluster 3 sites) (Fig. S2*D*). We also noted a difference in sequence composition between cluster 1 and clusters 2 and 3 (Fig. S2*E*). The basis of their differential enrichment may reflect chromatin variation at these regions that are distinguished by the biochemical properties specific to organic or solid phase purification. Because we used published standard FAIRE datasets that were generated with a shorter sequencing read length (ENCODE, 36-bp reads), we asked whether the difference in read length could partially account for the variability in mapping and sequence content at clusters 1 and 3 (Fig. S2*F*). Repeating these analyses after truncating the HT-FAIRE sequencing reads to 36 bp did not change the hierarchical clustering or histone modification associations (Fig. S2 *G* and *H*). Taken together, these data demonstrate that HT-FAIRE performs similarly to standard FAIRE and identifies regions that are biologically meaningful.

Application of HT-FAIRE to Small Molecule Screening. We then adapted HT-FAIRE for high-throughput automation and applied it in a targeted screen. The screen was based on two regions selected from a set of Ewing sarcoma-specific sites that we had previously shown were accessible in multiple Ewing sarcoma cell lines with accessibility that was dependent on continued expression of EWSR1-FLI1 (17). Regions that consistently demonstrate FAIRE enrichment or lack of enrichment across many cell types were included as controls (see Table S3).

We performed the screen using a custom library that consisted of 640 small molecules, including those designed to target histone methyltransferases, methyl lysine reader proteins, histone demethylases and deacetylases, DNA methyltransferases, and acetyl-lysine reader proteins. The compound collection included well-annotated molecular profiles (chemical probes) (25), as well as compounds that were designed around several chemical scaffolds originally directed toward specific targets of interest (methyl-lysine readers and transferases). The latter compounds have only been tested in vitro for activity on the proteins for which they were designed and likely have effects on other molecular targets. We hypothesized that the inclusion of a large number of uncharacterized compounds would increase the potential to identify previously unanticipated protein targets.

After optimizing conditions for growth and DMSO tolerance (Fig. S3), Ewing sarcoma patient-derived cells (EWS894) were exposed to 10 μM of each compound (or DMSO control) for 16 h in a 96-well format. The unit automation pipeline separated each of two 384-well compound plates containing the library into four 96-well plates for screening (Fig. S4). After application of HT-FAIRE, chromatin from the 96-well plates was combined into a 384-well plate format for qPCR-based testing of the signature and control regions in two technical replicates. The positive control region demonstrated a significant difference in FAIRE signal over the background control (plate 1, $P = 7.50e{-}53$; plate 2, $P = 6.63e{-}98$). Critically, signals from each of the disease-specific regions were highly concordant (Pearson $r = 0.8764$), which supported combining the values from both sites for subsequent analytics (Fig. 2*A*).

To quantify the degree to which chromatin accessibility changed after compound treatment, we calculated a "relative chromatin inhibition" (RCI) score that compared the relative enrichment at the oncogene-targeted regions with that at the positive control region. An RCI score of 1.0 was considered "no change." Compounds that similarly affected both the oncogene-targeted and control regions were considered nonspecific. DMSO (vehicle) and UNC0638 (10) (a chemical probe that we had previously determined not to affect aberrantly open chromatin in Ewing sarcoma cells) demonstrated an RCI of 1.0 (Fig. 2*B* and Fig. S5*A*). Because this primary screen was based on a single measurement, we permitted greater intersample variability, defining compounds with an RCI value greater than two SDs from the mean RCI score for

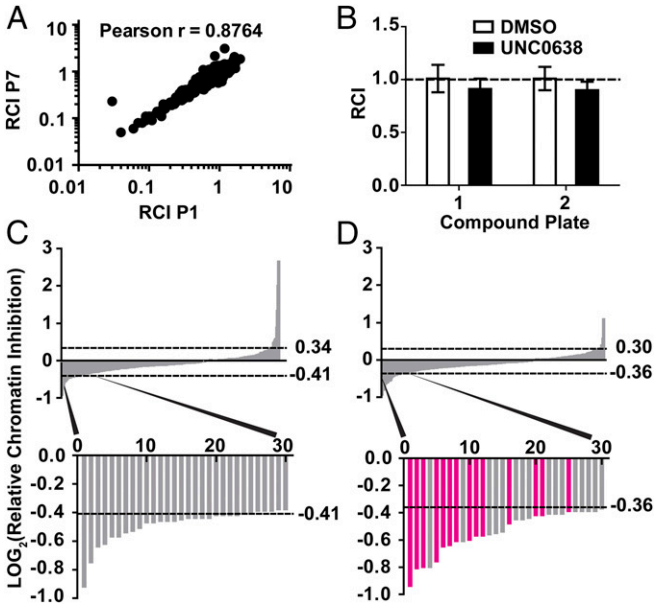

Fig. 2. Chromatin signature-based screen identified a cluster of HDAC inhibitors that significantly decreased EWSR1-FLI1–dependent chromatin accessibility. (*A*) The LOG_{10}-transformed relative chromatin inhibition (RCI) scores for the Ewing sarcoma-specific P1 and P7 regions are plotted (Pearson $r = 0.8764$). (*B*) RCI scores for DMSO and a negative control compound, UNC0638, are plotted for each 384-well plate. An RCI score of 1.0 indicates no change (dotted line). Error bars are the SD of 16 replicates. (*C* and *D*) Plate 1 (*C*) or plate 2 (*D*) LOG_2 ratio of the RCI values was plotted against the rank order of compounds from greatest relative decrease (*Top*, left side of *x* axis) to the greatest relative increase (*Top*, right side of *x* axis) in FAIRE signal. The dashed lines indicate the significance cutoff of RCI values ≥2 SDs or ≤2 SDs from the average RCI for DMSO controls. Thirty compounds that show the greatest decrease in FAIRE signal for each plate are magnified (*Bottom* graph). The bars representing HDAC inhibitors are highlighted in magenta.

DMSO-treated controls as "hits" (Fig. 2*B* and Fig. S5*A*) (26). Fifty-eight compounds met criteria for reduced chromatin accessibility (Fig. 2 *C* and *D*). Forty-three of these compounds were uncharacterized, 14 of which were analogs within a single chemical scaffold, and 15 were characterized chemical probes. Treatment with 20 compounds resulted in increased FAIRE signals, all of which were uncharacterized (Table S1). Because the goal of this study was to inhibit EWSR1-FLI1–mediated aberrant chromatin accessibility, we focused on those compounds that decreased the FAIRE signal.

We prepared a secondary screen plate that contained all hit compounds and 16 compounds that failed to show a change in chromatin accessibility in the initial screen (RCI of 1.0, no change). This secondary screen was performed on three independent replicates of EWS894 cells, permitting a more stringent threshold of 3 SDs from the mean RCI score to define hits (26, 27). Fifteen compounds (26%) met this enhanced threshold (Fig. 3*A* and Fig. S5*B*).

Remarkably, of the 21 HDAC inhibitors that were included in our library, 14 of these compounds scored as hits in both the primary and secondary screens (Fig. 3*A*). We compared the specificity of the active and inactive HDAC inhibitors (Table S2). Although the majority of the inhibitors in our set have known activity against multiple HDAC proteins, making it difficult to identify the specific HDAC target, inhibitors selective for HDAC6 (Tubastatin) (28) and HDAC8 (PCI-34051) (29) did not score in our screen, making it unlikely that either of these HDAC proteins is involved in maintaining aberrant chromatin accessibility in Ewing sarcoma. The overall reproducibility of the screen confirms the robustness of HT-FAIRE as an approach for discovering biologically relevant compounds using a small, focused compound library. A priori selection of inhibitors of HDAC proteins as lead candidates for screening would have been unlikely because histone hyperacetylation is commonly associated with destabilized nucleosomes and open chromatin.

To replicate the results of the screen, we focused on two hit compounds, Vorinostat and Panobinostat because these hydroxamate derivatives inhibit multiple classes of HDACs and have received FDA approval for oncological indications (30). Treatment of EWS894 cells with either of these compounds followed by HT-FAIRE resulted in a dose-dependent decrease in chromatin accessibility (Fig. S6*A*). This decrease was not observed with an HDAC inhibitor that did not score as a hit in our screen (Tubastatin), or a compound with an unrelated structure and protein target.

We then validated the compounds that emerged from our screen using standard FAIRE. FAIRE signals from cells treated with Panobinostat decreased at the test regions to a similar extent (approximately twofold) to that observed in the screen and also demonstrated a similar effect on two additional EWSR1-FLI1–targeted sites (Fig. 3*B*). Critically, positive control regions remained unaffected, demonstrating that the decreased RCI was not the result of increased signals at the control regions. We then validated the effect of additional HDAC inhibitors by standard FAIRE. Panobinostat, Vorinostat, and AR-42 demonstrated a similar magnitude effect on chromatin (Fig. 3*C*). Panobinostat also led to a dose-dependent decrease in FAIRE signal at an EWSR1-FLI1–targeted site (Fig. 3*D*). As further validation, we performed FAIRE-qPCR in two additional patient-derived EWSR1-FLI1–expressing Ewing sarcoma cell lines, EWS502 (Fig. S6*B*) and RD-ES (Fig. S6*C*). Panobinostat treatment significantly decreased FAIRE signals at EWSR1-FLI1 binding sites in both of these cell lines. Together, these data confirm that HDAC inhibitors are associated with reduced chromatin accessibility at EWSR1-FLI1–targeted regions as measured by both HT-FAIRE and standard FAIRE.

To explore the mechanism underlying the chromatin signature reversal, we asked whether EWSR1-FLI1 levels were affected by HDAC inhibitor treatment. Panobinostat and Vorinostat treatment resulted in a dose-dependent decrease in *EWSR1-FLI1* mRNA levels whereas Tubastatin had no effect (Fig. 4*A*). Consistent with the decrease in mRNA, EWSR1-FLI1 protein levels were also decreased after treatment with Panobinostat and Vorinostat

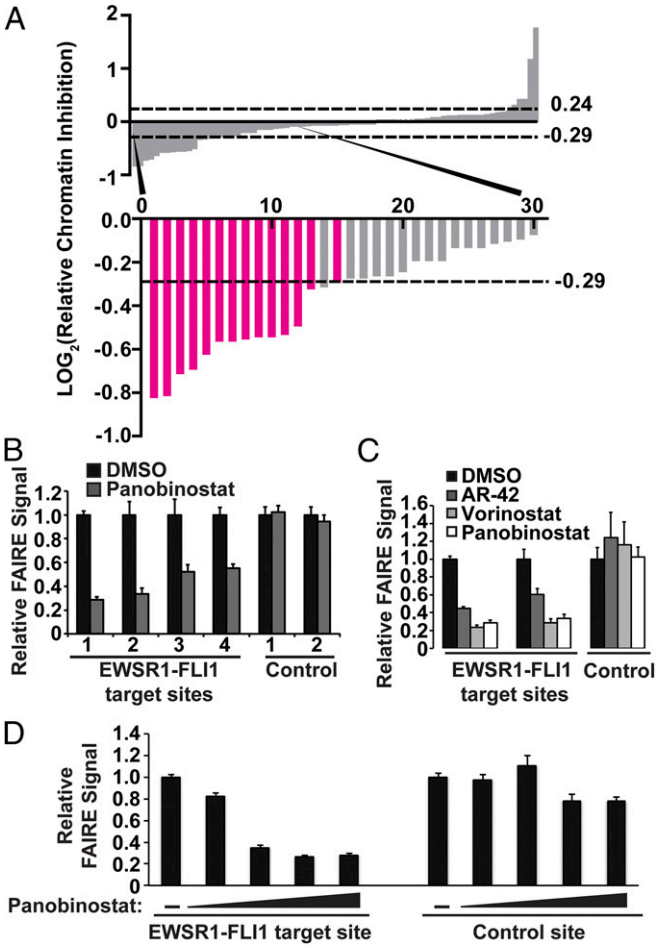

Fig. 3. HDAC inhibitors affect EWSR1-FLI1 chromatin accessibility in a dose-dependent manner. (*A*) Secondary screen that included all hit compounds from plate 1 and plate 2 and a selection of compounds that did not score. LOG_2 ratio of the RCI values as described for Fig. 2 *C* and *D*. The dashed lines indicate the significance cutoff of RCI values ≥3 SDs or ≤3 SDs from the average RCI for vehicle-treated controls. The bars representing HDAC inhibitors are highlighted in magenta. (*B*) Standard FAIRE-qPCR was performed on EWS894 cells treated with Panobinostat for EWSR1-FLI1 target sites (1, P1; 2, P7; 3, target 3; 4, target 4) (Table S3) and control sites (1, AURKAIP1; 2, control 2) (Table S3). (*C*) Standard FAIRE-qPCR (target sites P1, P7; control site AURKAIP1) was performed on EWS894 cells treated with Vorinostat, AR-42, or Panobinostat. (*D*) FAIRE-qPCR was performed on an EWSR1-FLI1 binding site (P1) and a control site (AURKAIP1) after treatment of EWS894 cells with DMSO or 10-fold dilutions of Panobinostat (10 μM to 0.01 μM). All treatments were 10 μM for 16 h unless otherwise noted. FAIRE is plotted relative to DMSO control, and error bars represent the SD of three replicates.

(Fig. 4*B*). Tubastatin did not affect EWSR1-FLI1 protein levels although a slight overall decrease was noted at 10 μM (Fig. 4*B*). These data suggest that Panobinostat and Vorinostat, both hit compounds identified in the HT-FAIRE screen, decrease levels of EWSR1-FLI1 by altering transcription.

We then asked whether ectopically expressed EWSR1-FLI1 would be similarly affected by HDAC inhibition. We generated a Ewing sarcoma cell line in which the endogenous EWSR1-FLI1 was silenced with concurrent stable expression of lentivirally transduced EWSR1-FLI1. Panobinostat or Vorinostat treatment of these cells did not affect *EWSR1-FLI1* mRNA levels (Fig. 4*C*). Correspondingly, treatment with multiple HDAC inhibitors had virtually no effect on exogenous EWSR1-FLI1 protein levels (Fig. 4*D*), in contrast to the endogenous protein (Fig. S7*A*). These data demonstrate that HDAC inhibition acts through transcription of the *EWSR1-FLI1* without affecting protein stability.

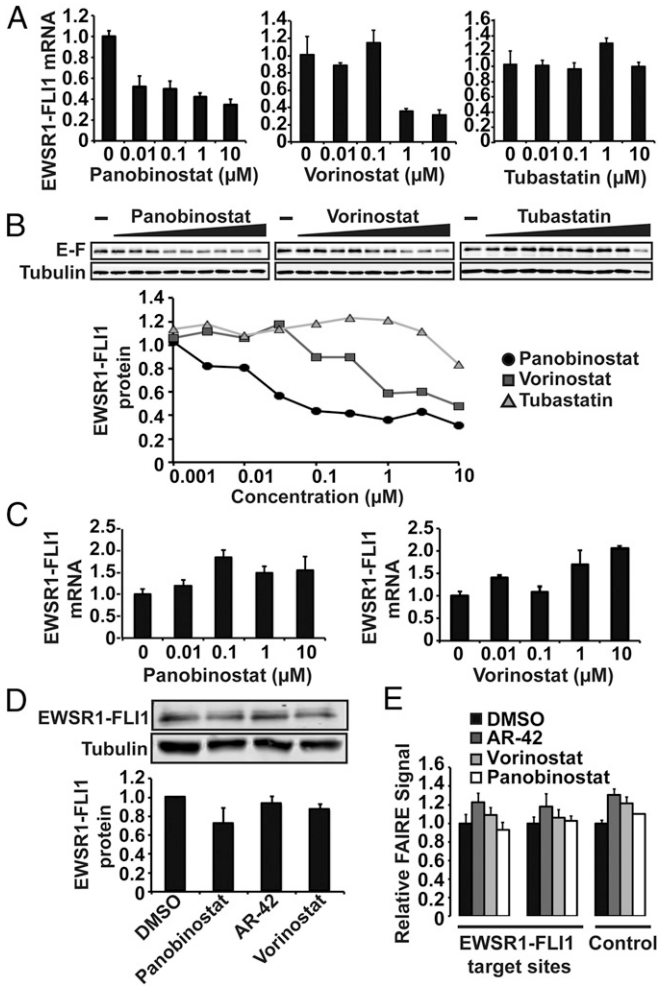

Fig. 4. EWSR1-FLI1 mRNA and protein levels are decreased after HDAC inhibition. (*A*) EWSR1-FLI1 mRNA levels were measured by qRT-PCR after treatment of EWS894 cells with indicated concentrations of Panobinostat, Vorinostat, or Tubastatin. (*B*) EWS894 cells were treated with varying concentrations of Panobinostat, Vorinostat, or Tubastatin (threefold dilutions, 10 μM to 0.001 μM). Cell extracts were assayed for EWSR1-FLI1 ("E-F") and tubulin protein levels by immunoblot. All treatments were for 16 h. (*C*) EWS894 cells lentivirally transduced with EWSR1-FLI1 were treated with varying concentrations of Panobinostat or Vorinostat. RNA was measured by qRT-PCR. (*D*) Transduced EWSR1-FLI1 protein levels were measured in EWS894 cells after treatment with HDAC inhibitors (10 μM) by immunoblotting. (*E*) FAIRE-qPCR measuring chromatin accessibility in EWS894 cells with exogenous EWSR1-FLI1 after treatment with 10 μM multiple HDAC inhibitors. All treatments were for 16 h. Error bars represent the SD of three technical replicates (*C* and *E*) or three biological replicates (*D*).

We then tested chromatin accessibility in the EWSR1-FLI1–transduced Ewing sarcoma cells. Treatment with multiple HDAC inhibitors failed to affect FAIRE signals at oncogene-targeted regions (Fig. 4*E*). These results were replicated in a second Ewing sarcoma cell line (EWS502) that similarly ectopically expresses EWSR1-FLI1 (Fig. S7*B*). Taken together, these data suggest that the loss of chromatin accessibility at EWSR1-FLI1 binding sites results from HDAC inhibition-mediated alteration in EWSR1-FLI1 transcription, thereby suppressing oncoprotein levels, rather than HDAC activity directly on chromatin at target sites.

Discussion

In contrast to previous efforts to inhibit EWSR1-FLI1 activity that have capitalized on individual target gene expression or physical interactions (31–36), the application of HT-FAIRE offered a strategy to identify therapeutics based on variation in chromatin accessibility, a universal genomic feature determined by the combined effects of transcriptional regulators and chromatin regulatory proteins (37). Indeed, FAIRE has been shown to detect specific chromatin changes resulting from treatment with anthracyclines that directly interact with DNA (38, 39), thereby demonstrating the utility of this assay to explore the function of small molecule compounds. Unlike chromatin immunoprecipitation (ChIP), FAIRE does not depend on the prior selection of a specific target. Without the need for an enzymatic processing step, FAIRE does not require the optimization (and consequent variability) associated with DNase, MNase, or Assay for Transposase-Accessible Chromatin (ATAC) (40), other techniques that explore chromatin accessibility. A specific chromatin signature associated with multiple molecular mechanisms can form the basis for an HT-FAIRE functional screen.

The identification of HDAC inhibitors was unanticipated because the screen sought to identify compounds associated with a selective decrease in chromatin accessibility, a feature associated with histone hypoacetylation. The unexpected outcome highlights an advantage of functionally screening a broad compound library to identify molecules that act directly and indirectly. We found that HDAC inhibitors decreased EWSR1-FLI1 levels, which explained the decreased accessibility of chromatin at targeted microsatellite repeat regions. The connection between HDAC activity and Ewing sarcoma has been noted previously. Romedepsin had been shown to decrease *EWSR1-FLI1* mRNA levels (41), and Romedepsin, Vorinostat, and Entinostat exhibited anti-proliferative activity on Ewing cells (41, 42). In addition, Vorinostat treatment reversed the EWSR1-FLI1–mediated transcriptional repressive signature in Ewing sarcoma cells (43). Each of the HDAC inhibitors previously associated with effects on Ewing sarcoma were identified in our screen.

The exact role of HDAC inhibitors on *EWSR1-FLI1* transcription is not understood. HDAC activity in transcription is complex because HDAC proteins can have both histone and nonhistone protein targets, can function as the catalytic subunits of multiple corepressor complexes including Sin3A, NuRD, NCoR/SMRT, and CoREST (44, 45), and are known to function in transcriptional elongation, which may selectively affect highly expressed genes in cancers (46, 47). Because HDAC inhibitors often target multiple HDAC proteins, each with variable potency, they can result in a pleiotropic effect on cellular pathways, making specific effects challenging to interpret. The selective HDAC inhibitors in our library targeted HDAC6 (Tubastatin) (28) or HDAC8 (PCI-34051) (29) and did not alter the Ewing chromatin signature in our screen (Table S2). For the pan-HDAC inhibitors that failed to decrease Ewing FAIRE signals, it is possible that the concentrations used were insufficient to inhibit the relevant HDAC protein(s).

In conclusion, we developed an approach to screen compounds based on changes in chromatin. HT-FAIRE is applicable to any cellular model associated with a specific chromatin accessibility signature and offers a general strategy to disrupt the function of proteins lacking structure amenable to small molecule targeting or the absence of complete characterization of the biochemical pathways and partners. The chemical probes identified by this method can offer mechanistic insights into chromatin dysregulation in disease, can lead to the identification of valid molecular targets, and can serve as starting points for drug discovery efforts.

Methods

Cell Culture and Western Analysis. EWS894 and EWS502 cells (48) were cultured in RPMI-1640 supplemented with 15% (vol/vol) FBS and maintained at standard growth conditions of 37 °C and 5% CO_2. Proteins were extracted using 2× Laemmli buffer, were separated by SDS/PAGE, and were then transferred onto nitrocellulose and probed for EWSR1-FLI1 (ab15289; Abcam) or tubulin (T9026; Sigma) and fluorescent secondary antibodies and quantified (LiCor).

Standard FAIRE, HT-FAIRE, and RNA Extraction. FAIRE for sequencing was as follows: Replicate samples of chromatin from 2×10^7 cells were divided. Equal portions were used for standard FAIRE, as described (20), or HT-FAIRE, using a ChIP DNA clean and concentrate column (11-379; Zymo Research) as per the manufacturer's instructions. FAIRE DNA from both replicates was prepared as per the manufacturer's recommendations (TruSeq DNA Sample Prep Kit; Illumina), and 50-bp reads were sequenced (HiSeq 2000; Illumina) at the University of North Carolina High-Throughput Sequencing Facility. A detailed version of the automated, high-throughput FAIRE screen is outlined in *SI Methods*. Cells in a 96-well format were incubated for 16 h with compound or vehicle at a final concentration of 10 μM. After formaldehyde cross-linking, cells were sonicated in Lysis Buffer A (20). Input was collected from untreated cells in the first column of each plate, and FAIRE was performed on remaining samples using columns (D5207; Zymo Research). Relative chromatin inhibition was determined by performing qPCR on FAIRE and input samples. Primer sequences are listed in Table S3. RNA was extracted (74134; Qiagen) followed by cDNA synthesis (Superscript III; Invitrogen). Ten microliters of qPCR reactions (SYBR Green Mastermix; Bio-Rad or Biotool) were performed according to the manufacturers' instructions. qPCR for FAIRE and cDNA was performed (ViiA7 Real-Time PCR system; Applied Biosystems) and analyzed using the ΔΔCt method (49).

Analysis of Standard FAIRE and HT-FAIRE. Sequencing data were analyzed as described in ref. 37. A detailed description of the analyses is available in *SI Methods*.

ACKNOWLEDGMENTS. We thank J. Lieb, D. Kireev, L. James, and members of the I.J.D. laboratory for meaningful discussions, and J. Jin for the UNC0638 compound. These studies were supported by the Wide Open Charitable Foundation, the V Foundation for Cancer Research, National Institutes of Health (NIH) Grants R01CA166447 (to I.J.D.) and RC1GM090732 and R01GM100919 (to S.V.F.), the Carolina Partnership, and the University Cancer Research Fund, University of North Carolina at Chapel Hill. A.W. was supported in part by NIH Grants T32CA071341 and T32GM007092 and J.T. was supported in part by Reelin' for Research.

1. Plass C, et al. (2013) Mutations in regulators of the epigenome and their connections to global chromatin patterns in cancer. *Nat Rev Genet* 14(11):765–780.
2. Waldmann T, Schneider R (2013) Targeting histone modifications: Epigenetics in cancer. *Curr Opin Cell Biol* 25(2):184–189.
3. Kaniskan HÜ, Konze KD, Jin J (2015) Selective inhibitors of protein methyltransferases. *J Med Chem* 58(4):1596–1629.
4. Daigle SR, et al. (2013) Potent inhibition of DOT1L as treatment of MLL-fusion leukemia. *Blood* 122(6):1017–1025.
5. Knutson SK, et al. (2012) A selective inhibitor of EZH2 blocks H3K27 methylation and kills mutant lymphoma cells. *Nat Chem Biol* 8(11):890–896.
6. Konze KD, et al. (2013) An orally bioavailable chemical probe of the lysine methyltransferases EZH2 and EZH1. *ACS Chem Biol* 8(6):1324–1334.
7. McCabe MT, et al. (2012) EZH2 inhibition as a therapeutic strategy for lymphoma with EZH2-activating mutations. *Nature* 492(7427):108–112.
8. Qi W, et al. (2012) Selective inhibition of Ezh2 by a small molecule inhibitor blocks tumor cells proliferation. *Proc Natl Acad Sci USA* 109(52):21360–21365.
9. Liu F, et al. (2013) Discovery of an in vivo chemical probe of the lysine methyltransferases G9a and GLP. *J Med Chem* 56(21):8931–8942.
10. Vedadi M, et al. (2011) A chemical probe selectively inhibits G9a and GLP methyltransferase activity in cells. *Nat Chem Biol* 7(8):566–574.
11. James LI, et al. (2013) Discovery of a chemical probe for the L3MBTL3 methyllysine reader domain. *Nat Chem Biol* 9(3):184–191.
12. Filippakopoulos P, et al. (2010) Selective inhibition of BET bromodomains. *Nature* 468(7327):1067–1073.
13. Dawson MA, et al. (2011) Inhibition of BET recruitment to chromatin as an effective treatment for MLL-fusion leukaemia. *Nature* 478(7370):529–533.
14. Nicodeme E, et al. (2010) Suppression of inflammation by a synthetic histone mimic. *Nature* 468(7327):1119–1123.
15. Delattre O, et al. (1992) Gene fusion with an ETS DNA-binding domain caused by chromosome translocation in human tumours. *Nature* 359(6391):162–165.
16. Delattre O, et al. (1994) The Ewing family of tumors: A subgroup of small-round-cell tumors defined by specific chimeric transcripts. *N Engl J Med* 331(5):294–299.
17. Patel M, et al. (2012) Tumor-specific retargeting of an oncogenic transcription factor chimera results in dysregulation of chromatin and transcription. *Genome Res* 22(2):259–270.
18. Gangwal K, et al. (2008) Microsatellites as EWS/FLI response elements in Ewing's sarcoma. *Proc Natl Acad Sci USA* 105(29):10149–10154.
19. Consortium EP, et al.; ENCODE Project Consortium (2012) An integrated encyclopedia of DNA elements in the human genome. *Nature* 489(7414):57–74.
20. Simon JM, Giresi PG, Davis IJ, Lieb JD (2012) Using formaldehyde-assisted isolation of regulatory elements (FAIRE) to isolate active regulatory DNA. *Nat Protoc* 7(2):256–267.
21. Song L, et al. (2011) Open chromatin defined by DNaseI and FAIRE identifies regulatory elements that shape cell-type identity. *Genome Res* 21(10):1757–1767.
22. McLean CY, et al. (2010) GREAT improves functional interpretation of cis-regulatory regions. *Nat Biotechnol* 28(5):495–501.
23. De Val S, Black BL (2009) Transcriptional control of endothelial cell development. *Dev Cell* 16(2):180–195.
24. Meadows SM, Myers CT, Krieg PA (2011) Regulation of endothelial cell development by ETS transcription factors. *Semin Cell Dev Biol* 22(9):976–984.
25. Frye SV (2010) The art of the chemical probe. *Nat Chem Biol* 6(3):159–161.
26. Malo N, Hanley JA, Cerquozzi S, Pelletier J, Nadon R (2006) Statistical practice in high-throughput screening data analysis. *Nat Biotechnol* 24(2):167–175.
27. Caraus I, Alsuwailem AA, Nadon R, Makarenkov V (2015) Detecting and overcoming systematic bias in high-throughput screening technologies: A comprehensive review of practical issues and methodological solutions. *Brief Bioinform* 16(6):974–986.
28. Butler KV, et al. (2010) Rational design and simple chemistry yield a superior, neuroprotective HDAC6 inhibitor, tubastatin A. *J Am Chem Soc* 132(31):10842–10846.
29. Balasubramanian S, et al. (2008) A novel histone deacetylase 8 (HDAC8)-specific inhibitor PCI-34051 induces apoptosis in T-cell lymphomas. *Leukemia* 22(5):1026–1034.
30. Falkenberg KJ, Johnstone RW (2014) Histone deacetylases and their inhibitors in cancer, neurological diseases and immune disorders. *Nat Rev Drug Discov* 13(9):673–691.
31. Stegmaier K, et al. (2007) Signature-based small molecule screening identifies cytosine arabinoside as an EWS/FLI modulator in Ewing sarcoma. *PLoS Med* 4(4):e122.
32. Erkizan HV, et al. (2009) A small molecule blocking oncogenic protein EWS-FLI1 interaction with RNA helicase A inhibits growth of Ewing's sarcoma. *Nat Med* 15(7):750–756.
33. Sankar S, et al. (2014) Reversible LSD1 inhibition interferes with global EWS/ETS transcriptional activity and impedes Ewing sarcoma tumor growth. *Clin Cancer Res* 20(17):4584–4597.
34. Owen LA, Kowalewski AA, Lessnick SL (2008) EWS/FLI mediates transcriptional repression via NKX2.2 during oncogenic transformation in Ewing's sarcoma. *PLoS One* 3(4):e1965.
35. Boro A, et al. (2012) Small-molecule screen identifies modulators of EWS/FLI1 target gene expression and cell survival in Ewing's sarcoma. *Int J Cancer* 131(9):2153–2164.
36. Kovar H (2014) Blocking the road, stopping the engine or killing the driver? Advances in targeting EWS/FLI-1 fusion in Ewing sarcoma as novel therapy. *Expert Opin Ther Targets* 18(11):1315–1328.
37. Simon JM, et al. (2014) Variation in chromatin accessibility in human kidney cancer links H3K36 methyltransferase loss with widespread RNA processing defects. *Genome Res* 24(2):241–250.
38. Pang B, de Jong J, Qiao X, Wessels LF, Neefjes J (2015) Chemical profiling of the genome with anti-cancer drugs defines target specificities. *Nat Chem Biol* 11(7):472–480.
39. Pang B, et al. (2013) Drug-induced histone eviction from open chromatin contributes to the chemotherapeutic effects of doxorubicin. *Nat Commun* 4:1908.
40. Tsompana M, Buck MJ (2014) Chromatin accessibility: A window into the genome. *Epigenetics Chromatin* 7(1):33.
41. Sakimura R, et al. (2005) Antitumor effects of histone deacetylase inhibitor on Ewing's family tumors. *Int J Cancer* 116(5):784–792.
42. Sonnemann J, et al. (2007) Histone deacetylase inhibitors induce cell death and enhance the apoptosis-inducing activity of TRAIL in Ewing's sarcoma cells. *J Cancer Res Clin Oncol* 133(11):847–858.
43. Sankar S, et al. (2013) Mechanism and relevance of EWS/FLI-mediated transcriptional repression in Ewing sarcoma. *Oncogene* 32(42):5089–5100.
44. Singh BN, et al. (2010) Nonhistone protein acetylation as cancer therapy targets. *Expert Rev Anticancer Ther* 10(6):935–954.
45. Delcuve GP, Khan DH, Davie JR (2013) Targeting class I histone deacetylases in cancer therapy. *Expert Opin Ther Targets* 17(1):29–41.
46. Kim YJ, et al. (2013) HDAC inhibitors induce transcriptional repression of high copy number genes in breast cancer through elongation blockade. *Oncogene* 32(23):2828–2835.
47. Yokoyama S, et al. (2008) Pharmacologic suppression of MITF expression via HDAC inhibitors in the melanocyte lineage. *Pigment Cell Melanoma Res* 21(4):457–463.
48. Patel M, et al. (2014) PTEN deficiency mediates a reciprocal response to IGFI and mTOR inhibition. *Mol Cancer Res* 12(11):1610–1620.
49. Livak KJ, Schmittgen TD (2001) Analysis of relative gene expression data using real-time quantitative PCR and the 2(-Delta Delta C(T)) Method. *Methods* 25(4):402–408.
50. Thurman RE, et al. (2012) The accessible chromatin landscape of the human genome. *Nature* 489(7414):75–82.
51. Zhang Y, et al. (2008) Model-based analysis of ChIP-Seq (MACS). *Genome Biol* 9(9):R137.
52. Rozowsky J, et al. (2009) PeakSeq enables systematic scoring of ChIP-seq experiments relative to controls. *Nat Biotechnol* 27(1):66–75.
53. Heinz S, et al. (2010) Simple combinations of lineage-determining transcription factors prime cis-regulatory elements required for macrophage and B cell identities. *Mol Cell* 38(4):576–589.

Supporting Information

Pattenden et al. 10.1073/pnas.1521827113

SI Methods

Analysis of Standard FAIRE and HT-FAIRE. FAIRE data from seven cell lines (H1-hESC, HeLa, HepG2, NHEK, K562, GM12878, and HUVEC) were generated previously (50). For all signal-based analyses, one replicate was used for all cell lines except HUVEC, for which data from both replicates were used in parallel. Published sets of FAIRE sites were used in all cases. For HT-FAIRE, data from both replicates were combined, and one set of FAIRE sites was called using MACS2 (51) with a shift size set to 100. For hierarchical clustering analyses, we computed normalized FAIRE signal in 500-bp nonoverlapping windows across the genome. Windows were first filtered for those with an average signal greater than 0.25 (581,514 windows remained) and that fell within an expected range (580,605 windows remained). Windows exhibiting a wide variation across samples (SD greater than 0.5; 9,711 windows remained) were then selected. Signal in these windows was then median-centered and hierarchically clustered using average linkage. ChIP-seq data for histone modifications and transcription factors, as well as DNase hypersensitivity, were generated previously (50). Repetitive element classes were as defined by RepeatMasker, and genomic redundancy was computed for 36- and 50-bp reads using PeakSeq (52). Motifs in clusters 1–3 were identified using HOMER (53) using the 500-bp flanking sequence as background. Motifs were considered significant if they had a q-value equal to 0, they occurred in >20% of the target sequences, and had a greater than threefold enrichment in the target sequences relative to flanking sequences (background). Motifs in the same transcription factor family were merged for simplicity of presentation.

Detailed Description of High-Throughput FAIRE Screen. The automated, high-throughput FAIRE screen was performed in a 96-well format. Compound and vehicle controls were used in the assay at a final concentration of 10 μM in 0.1% DMSO in cell culture media. Compounds were plated onto a 96-well V-bottom cell culture plate (651180; Greiner Bio-One), and EWS894 cells were added (Multidrop Titertek) at 1×10^5 cells per well in a 100-μL final volume of cell culture media (RPMI supplemented with 15% FBS). Cells were incubated with compound for 16 h at 37 °C and 5% CO_2 and then harvested. Formaldehyde diluted in cell culture media to a final concentration of 1% per well was added (Multidrop Titertek). Plates were incubated for 5 min at 37 °C and 5% CO_2, followed by addition of glycine to a final concentration of 125 mM and incubation at room temperature for 5 min. Plates were centrifuged for 5 min at 500 × *g* (5810R centrifuge; Eppendorf) to pellet the cells. Media were removed by quickly inverting the plate. Cells were washed once with PBS and pelleted. A Tecan Evo 200 was used for all subsequent liquid handling. Cells were suspended in 50 μL of Lysis buffer A (20) and transferred to a 0.2-mL 96-raised well PCR plate (27-105; Genesee Scientific) for sonication. The plates were sealed with a 96-well silicone sealing mat (22-513; Genesee Scientific), and a pin lid was pushed through the seal (SL0096-P21-SS; Matrical Bioscience). Plates were sonicated (SonicMan; Matrical Bioscience) for 20 cycles for 15 s at 60% power. Then, 700 U of RNase (2900142; 5 Prime) was added to each well and incubated for 5 min at room temperature. Untreated samples from the first column of the plate were removed and pooled for input DNA. The input sample was digested with 20 μg of proteinase K at 55 °C overnight and then purified by phenol-chloroform extraction. FAIRE was performed by transferring liquid from the remaining wells in columns 2–12 to a ZR-96 ChIP DNA silica matrix clean and concentrator column (D5207; Zymo Research). The column was then washed according to the manufacturer's instructions using a QiaVAC 96 (19504; Qiagen). DNA was eluted in a 100-μL Elution Buffer (Zymo Research). DNA was separated on a 1.5% agarose gel to confirm fragmentation. Ten microliters of the remaining input was diluted 1:1,000 and added back to the plate containing the FAIRE DNA. Buffer alone was also added to the plate as a control for qPCR. Two microliters of each sample was transferred from the 96-well plate to a 384-well plate for use in qPCR. Input samples were diluted 1:1,000, and FAIRE samples were diluted 1:100 in water for comparison of standard and HT-FAIRE. Input samples were diluted 1:1,000, and FAIRE samples (100-μL elution volume) were used undiluted for the HT-FAIRE screen. Two microliters of each diluted sample was subjected to quantification qPCR in duplicate on the ABI 7900HT using FastStart SYBR Green Master Mix ROX (Roche) in a 10-μL final volume. Primer sequences are listed in Table S3. Percent input was determined using the ΔCt method (49). For the comparison of phenol-chloroform and column-based FAIRE methods, ΔCt values were normalized to a genomic region near the PRPF31 gene that is negative for FAIRE signal. For the FAIRE screen, relative chromatin inhibition was calculated using the following equation: $(((\Delta\Delta Ct_{P1}/\Delta\Delta Ct_{AURKAIP1}) + (\Delta\Delta Ct_{P7}/\Delta\Delta Ct_{AURKAIP1}))/2)$, where P1 and P7 are EWSR1-FLI1–dependent open chromatin regions, AURKAIP1 is a region of chromatin that consistently has a positive FAIRE signal, and ΔΔCt is $(\text{FAIRE } Ct_{TREATED}/\text{Input } Ct_{TREATED})/(\text{FAIRE } Ct_{DMSO}/\text{Input } Ct_{DMSO})$.

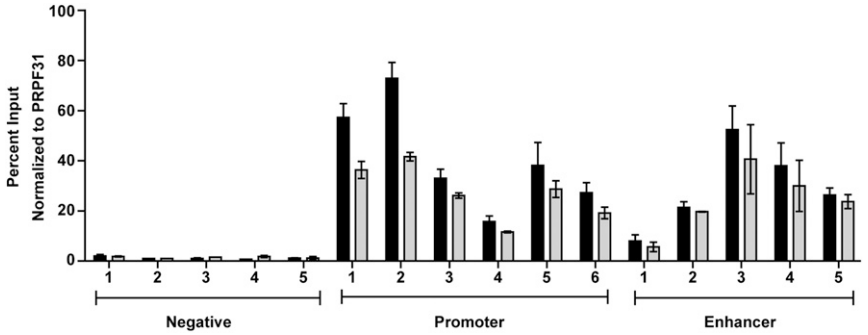

Fig. S1. Comparison of standard versus HT-FAIRE by quantitative PCR (qPCR). Chromatin was prepared from endothelial (HUVEC) cells and divided in half, and input was reserved. Each half was subjected to standard (black bars) or column-based (gray bars) FAIRE followed by qPCR. Primer sets included regions that are negative (Negative) for FAIRE signal, promoter regions (Promoter) from actively transcribed genes, and enhancer regions (Enhancer) (Table S3). Percent input (ΔCt) values were normalized to a genomic region near the PRPF31 gene that is negative for FAIRE signal. Error bars represent the SE of two biological replicates with two technical replicates each.

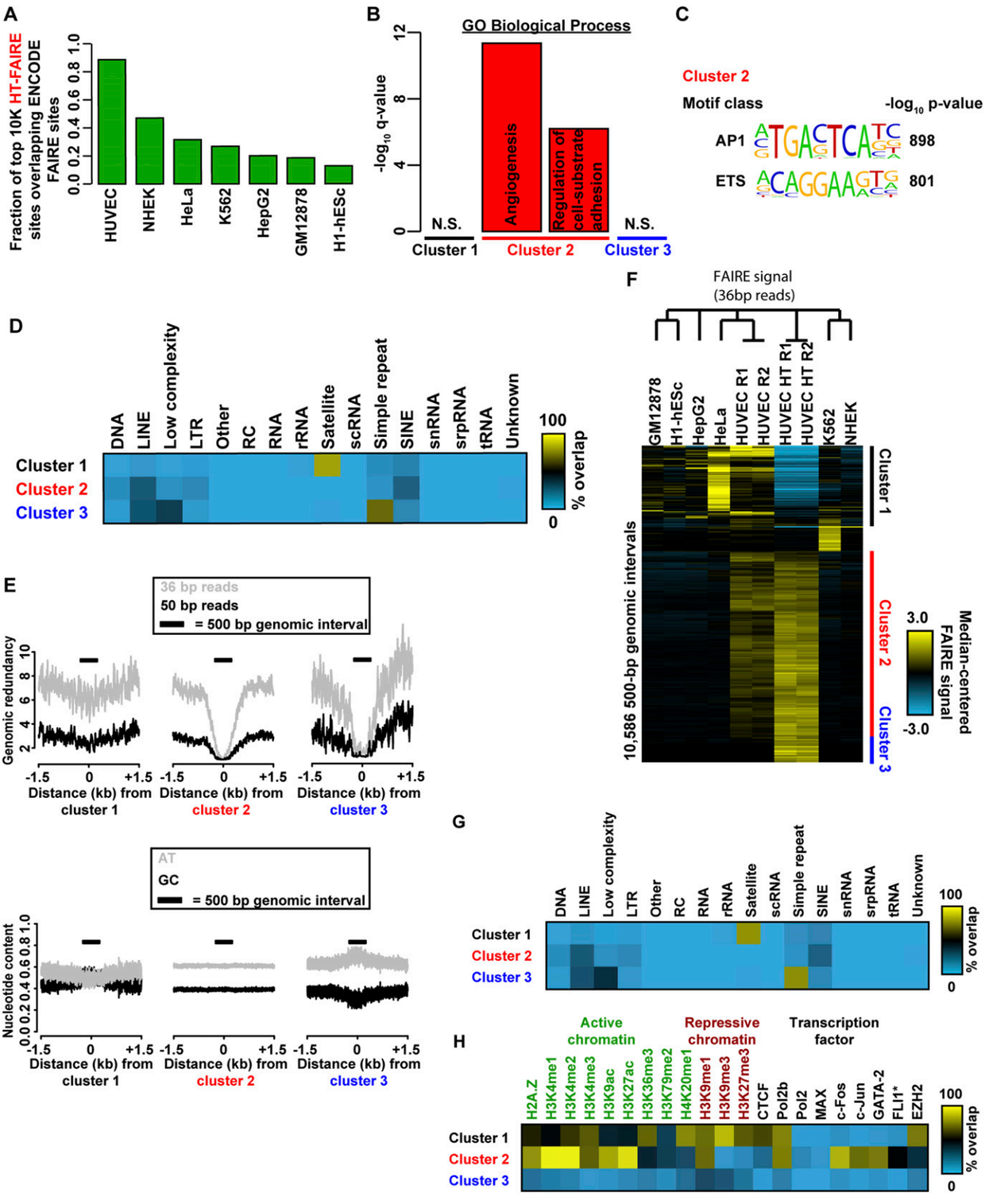

Fig. S2. Comparison of FAIRE methodologies. (*A*) Fraction of top 10,000 HT-FAIRE enriched sites overlapping standard FAIRE sites from HUVEC and six other cell types (ENCODE). (*B*) Ontology enrichment (GREAT) of genes associated with sites in clusters 1–3 (Fig. 1*E*). (*C*) Highly enriched TF motifs in cluster 2. Clusters 1 and 3 did not have any motifs determined to be significant by a multicomponent test (*Methods*). (*D*) Mappability (*Left*) and nucleotide content (*Right*) within 1.5 kb of sites from clusters 1–3 (Fig. 1*E*). Mappability was assessed for both 36- and 50-bp reads. Genomic redundancy refers to the number of times a given 36- or 50-mer occurs in the reference genome. 500 bp window indicated by bar. (*E*) Fractional overlap annotation of clusters 1–3 (Fig. 1*E*) with repetitive element classes. (*F*) Fractional overlap annotation of clusters 1–3 (*H*) with histone modifications and transcription factor ChIP-seq peak calls (ENCODE). (*G*) Fractional overlap annotation of clusters 1–3 (H) with repetitive element classes (RepeatMasker). (*H*) Hierarchical clustering analysis of ENCODE FAIRE signal in 500-bp intervals from seven cell types, as well as HUVEC HT-FAIRE after truncation of 50-bp reads to 36 bp. Identified clusters exhibit method specificity (clusters 1 and 3) and cell-type specificity (cluster 2).

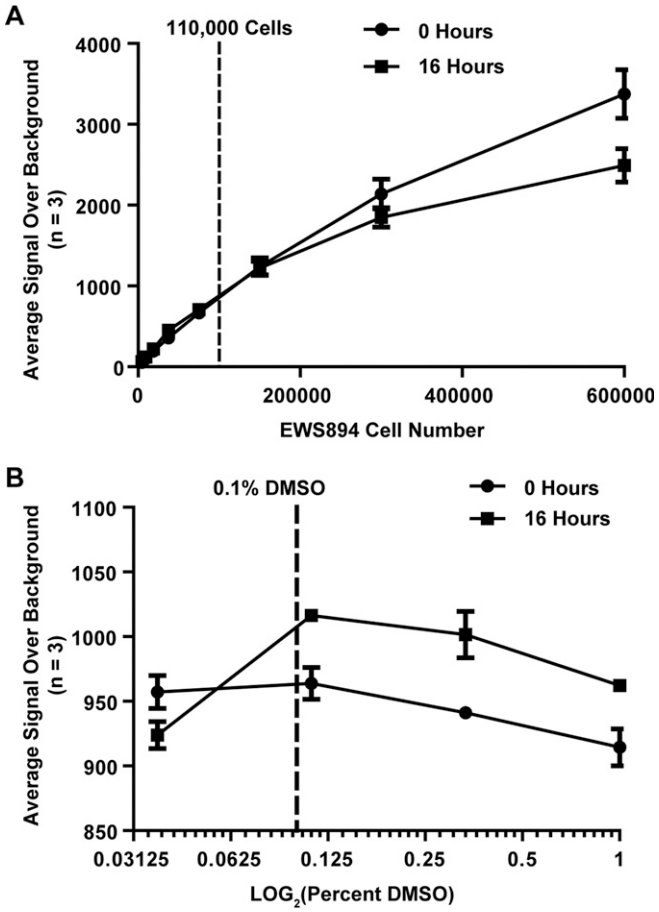

Fig. S3. EWS894 cell number and DMSO tolerance for HT-FAIRE assay. (*A*) Assay showing cell viability at increasing cell density in a 96-well plate after 16-h incubation. A plating density of 1.1×10^5 cells per well was selected for the assay (dotted line). The *x* axis shows cell number. The *y* axis shows the average luminescent signal over background (media only). Error bars represent the SD of three replicates. (*B*) Assay showing cell viability after 16-h treatment of 1.1×10^5 EWS894 cells per well with twofold dilutions of DMSO ranging from 1% to 0.03125%. Cells begin to lose viability at DMSO concentrations higher than 0.1% (dotted line). The *x* axis shows the LOG_2-transformed percent DMSO concentration. The *y* axis shows the average luminescent signal over background (no DMSO). Error bars represent the SD of three replicates.

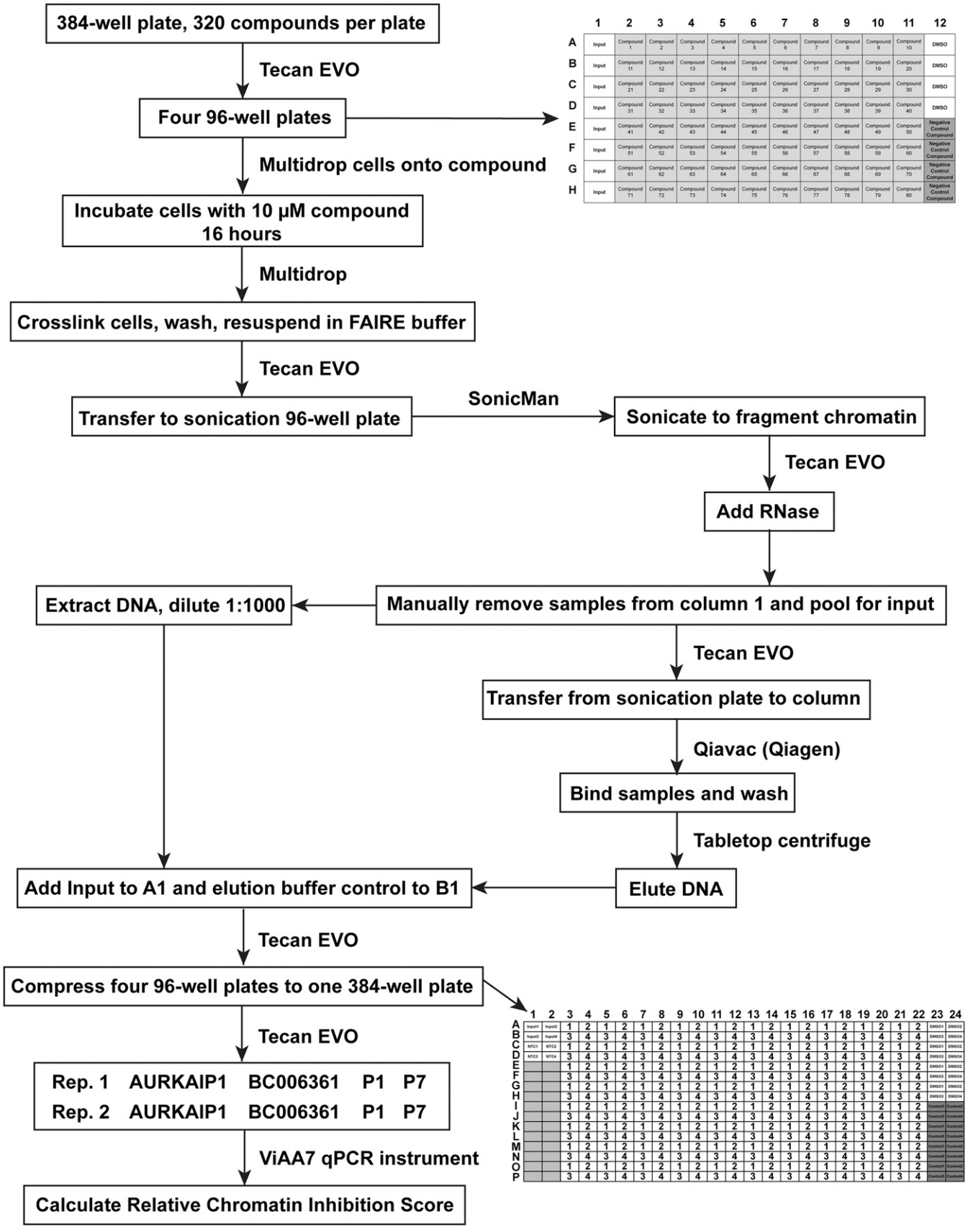

Fig. S4. Flowchart outlining the automation steps for HT-FAIRE.

A

Plate	Relative Chromatin Inhibition		
	Average DMSO Value	Standard Deviation	Cutoff for 2 SD
1	1.01	0.13	0.75
2	1.01	0.11	0.78

B

Plate	Relative Chromatin Inhibition		
	Average DMSO Value	Standard Deviation	Cutoff for 3 SD
Hits	1.00	0.03	0.91

Fig. S5. Cutoff values for HT-FAIRE screen hits. (*A*) Compounds were assigned as a hit for the HT-FAIRE screen if they had an RCI score of ≤2 SDs from the average DMSO RCI score. (*B*) Compounds were assigned as a hit in the HT-FAIRE secondary screen if they had an RCI score of ≤3 SDs form the average DMSO RCI score.

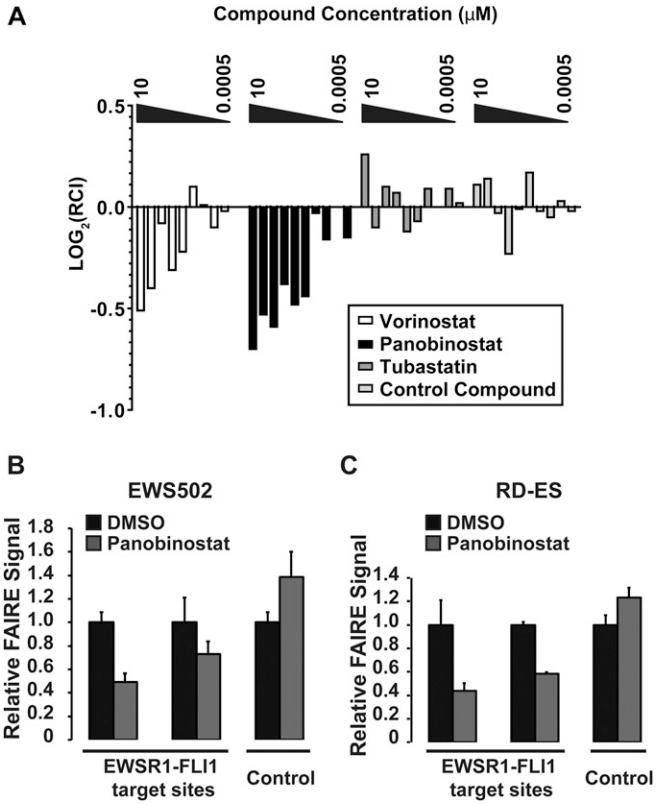

Fig. S6. HDAC inhibition selectively decreases chromatin accessibility at EWSR1-FLI1 binding sites. (*A*) HT-FAIRE-qPCR at the same genomic regions used for the original screen was conducted after treatment of EWS894 cells for 16 h with threefold dilutions of Vorinostat, Panobinostat, Tubastatin, or a control compound in concentrations ranging from 10 to 0.0005 μM. Error bars represent the SE of two biological replicates with two technical replicates each. FAIRE-qPCR at EWSR1-FLI1 target sites and control site after Panobinostat treatment of (*B*) EWS502 or (*C*) RD-ES cells. EWSR1-FLI1 targets sites were P1 and P7 for *B* and *C*. Control FAIRE site was AURKAIP1 for *B* and *C*. All treatments were at 10 μM for 16 h unless otherwise noted. FAIRE is plotted relative to DMSO control and error bars represent the SD of three replicates.

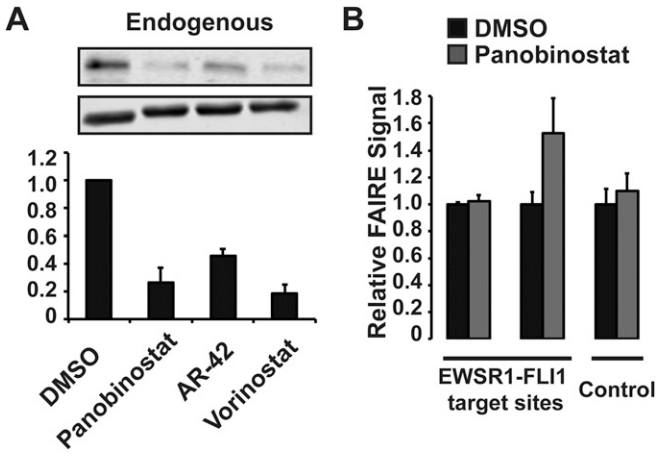

Fig. S7. Chromatin effects of HDAC inhibition are dependent on HDAC-mediated transcriptional changes. (*A*) Endogenous EWSR1-FLI1 protein levels were measured in EWS894 cells after treatment with HDAC inhibitors (10 μM) by immunoblotting. (*B*) FAIRE-qPCR EWS502 cells with exogenous EWSR1-FLI1 treated with 10 μM Panobinostat. EWSR1-FLI1 targets sites were P1 and P7, and control FAIRE site was AURKAIP1. All treatments were for 16 h. Error bars represent the SD of three biological replicates (*A*) or three technical replicates (*B*).

Table S1. Compounds that produced a statistically significant change in FAIRE signal

Plate	FAIRE signal	Target category	Chemical category	No. of hit compounds
1	Decrease	Methyl lysine reader	Uncharacterized	8
		DNA methyltransferase	Chemical probe	1
		Lysine methyltransferase	Uncharacterized	16
	Increase	Methyl lysine reader	Uncharacterized	6
		Lysine methyltransferase	Uncharacterized	6
2	Decrease	Histone deacetylase	Chemical probe (Table S2)	14
		Methyl lysine reader	Uncharacterized	10
		Lysine methyltransferase	Uncharacterized	6
		Arginine methyltransferase	Uncharacterized	3
	Increase	Methyl lysine reader	Uncharacterized	5
		Lysine methyltransferase	Uncharacterized	3

Hit compounds, their effect on FAIRE signal, and the number in each target category are listed.

Table S2. Histone deacetylase inhibitors included in the compound library

HDAC inhibitor	Hit?	HDAC target
Panobinostat (LBH-589)	Yes	HDAC1, HDAC2, HDAC3, HDAC6
AR-42 (HDAC-42)	Yes	Pan inhibitor
Trichostatin A (TSA)	Yes	Pan inhibitor
Vorinostat (SAHA)	Yes	HDAC1, HDAC2, HDAC3, HDAC6
Entinostat (MS-275)	Yes	HDAC1, HDAC2, HDAC3, HDAC9
Abexinostat (PCI-24781)	Yes	HDAC1, HDAC2, HDAC3, HDAC6, HDAC10
Dacinostat (NVP-LAQ824)	Yes	HDAC1, HDAC3, HDAC4, HDAC6
Quisinostat (JNJ-26481585)	Yes	Pan inhibitor
CUDC-101	Yes	Pan-HDAC, EGFR, HER2
Pracinostat (SB939)	Yes	Pan inhibitor
Givinostat (ITF2357)	Yes	HDAC1, HDAC2, HDAC3, HDAC4, HDAC6, HDAC7
CUDC-907	Yes	Pan-HDAC and PI3K
M344	Yes	Pan inhibitor
Romidepsin (FK228)	Yes	HDAC1, HDAC2, HDAC3, HDAC8
Tubastatin HCl	No (negative control)	HDAC6
Belinostat (PXD101)	No	HDAC1, HDAC2, HDAC3, HDAC6
Mocetinostat (MGCD0103)	No	HDAC1, HDAC2
Droxinostat	No	HDAC3, HDAC6, HDAC8
MC1568	No	HDAC4, HDAC5, HDAC7, HDAC9
PCI-34051	No	HDAC8
Tacedinaline (CI-994)	No	HDAC1, HDAC2, HDAC3

Histone deacetylase inhibitors, specification of screening status, and recognized HDAC target specificity are shown.

Table S3. Primers used for FAIRE- and RNA-quantitative PCR

Name	Oligo sequence
AURKAIP1 forward (positive control)	TATACCCGCAGGTCCAGAATCGTT
AURKAIP1 reverse (positive control)	AATAGCTCTAGACGCTTCCGCCTT
BC006361 forward (negative control)	TTCTCCAACTTTGGAAGCCCAGGA
BC006361 reverse (negative control)	TGTCTCCTTCTAGGCCCTCACAAT
P1 forward (EWSR1-FLI1 binding)	AAGGAAGGAAGGGAGGGACACATAC
P1 reverse (EWSR1-FLI1 binding)	CCTGTGAGTGTGACAGATTACTTGG
P7 forward (EWSR1-FLI1 binding)	GGGTGACAGAGTAAGATCCTGTCAGA
P7 reverse (EWSR1-FLI1 binding)	TGGGCGTGGTTCTCATGT
Enhancer1 forward	TCCTGACTCACTGCCTGGAGCAT
Enhancer1 reverse	GGGATTCCTGGAGTCACGGCA
Enhancer2 forward	GGCTCAAGCGCCTGGGTTTTGTA
Enhancer2 reverse	CAGCGTGGCTTCCTGGGCTTC
Enhancer3 forward	TTGCAAGTGAGTAAGCAGAAGCCCA
Enhancer3 reverse	AGCTGACCTCTCCCCTGTGTTAGT
Enhancer4 forward	AGTGTGGCGCCGCTCTGGTT
Enhancer4 reverse	CGTATTTGGCCACAGGAGGGAGC
Enhancer5 forward	ACGGCTGATCGTGTGACTTTCTGC
Enhancer5 reverse	GCCTTGACCAACTTGCTGAGGAGT
Negative1 forward	GTGGGAAGCTATGGCTGAGAAGCA
Negative1 reverse	TTGCCTTGGATTCCGTGCAGC
Negative2 forward	ACAGCCGGGGCAACTAGAAGA
Negative2 reverse	GACACCGCTTGGACCCGAGG
Negative3 forward	CCAGCTTGTCATGGCTACAGGGC
Negative3 reverse	GCTCACCGCAGTGACTCAGCAG
Negative4 forward	AGGTCAGCGTCAAAGAGGGGCT
Negative4 reverse	ACCTGACGCATGAAGGGCAGC
Negative5 forward	AGAGCCAAACCCAAGGAGGTAACTA
Negative5 reverse	GCCCACATGCATGCAATCCCA
Promoter1 forward	CGGGAGGCCAATCGAACGCC
Promoter1 reverse	GCTGAACGTCGCTCCTGACCC
Promoter2 forward	GCACCTCCCTCTGCCGCTTC
Promoter2 reverse	GCCCTCAAAGGGGCGGAACC
Promoter3 forward	ACTGCGTCGCTGGCTTGGAG
Promoter3 reverse	AAACGCGTGCCCAGCCAATCA
Promoter4 forward	GGAACAGATGAGGCAGGCAGGG
Promoter4 reverse	TTCTTTCCTCCTCTTTTTGCGGTGG
Promoter5 forward	GTGAGAGTGCAGGGCCCCAAG
Promoter5 reverse	GCCCGCCTTTCTCGCCGGTA
Promoter6 forward	TCACATGACCCGCCCAACCG
Promoter6 reverse	CGACGGCGGAAGAGAACGCT
Target 3 forward	GCATCAGGAAGCCTGGATCCATTA
Target 3 reverse	GTATATACCAACACCCTTCCCTG
Target 4 forward	AGATCCGGTTCAAATGGCAAGAGC
Target 4 reverse	GCACTCATCCTTAAGCCTCAACCA
Control 2 forward	CAAACTTCGGCTCACTTCGGCAAT
Control 2 reverse	AAGAAAGCCGAAACATGTCGCTCC
EWSR1-FLI1 mRNA forward	GCTATGGTCAACAAAGCAGCTATG
EWSR1-FLI1 mRNA reverse	TTGGCTAGGCGACTGCTGGT
RPL27 mRNA forward	GACGCAAAGCTGTCATCGTG
RPL27 mRNA reverse	GCAGTTTCTGGAAGAACCAC